



Sampling Volcanic Plume Using a Drone-Borne SeIPS for Remotely Determined Stable Isotopic Compositions of Fumarolic Carbon Dioxide

Urumu Tsunogai^{1*}, Ryo Shingubara^{1†}, Yuhei Morishita¹, Masanori Ito¹, Fumiko Nakagawa¹, Shin Yoshikawa², Mitsuru Utsugi² and Akihiko Yokoo²

¹Graduate School of Environmental Studies, Nagoya University, Nagoya, Japan, ²Aso Volcanological Laboratory, Institute for Geothermal Sciences, Kyoto University, Kumamoto, Japan

OPEN ACCESS

Edited by:

Alessandro Aiuppa,
University of Palermo, Italy

Reviewed by:

Philipson Bani,
Laboratoire Magmas et Volcans
(LMV), France
John Stix,
McGill University, Canada

*Correspondence:

Urumu Tsunogai
urumu@nagoya-u.jp

†Present address:

Ryo Shingubara,
National Agriculture and Food
Research Organization (NARO),
Institute for Agro-Environmental
Sciences (NIAES), Tsukuba, Japan

Specialty section:

This article was submitted to
Volcanology,
a section of the journal
Frontiers in Earth Science

Received: 12 December 2021

Accepted: 28 February 2022

Published: 28 March 2022

Citation:

Tsunogai U, Shingubara R,
Morishita Y, Ito M, Nakagawa F,
Yoshikawa S, Utsugi M and Yokoo A
(2022) Sampling Volcanic Plume Using
a Drone-Borne SeIPS for Remotely
Determined Stable Isotopic
Compositions of Fumarolic
Carbon Dioxide.
Front. Earth Sci. 10:833733.
doi: 10.3389/feart.2022.833733

Both chemical and isotopic compositions of concentrated volcanic plumes are highly useful in evaluating the present status of active volcanoes. Monitoring their temporal changes is useful for forecasting volcanic eruptions as well. Recently, we developed a drone-borne automatic volcanic plume sampler, called SeIPS, wherein an output signal from a sulfur dioxide (SO₂) sensor triggered a pump to collect plume samples when the SO₂ concentration exceeded a predefined threshold. In this study, we added a radio transmission function to the sampler, which enabled our operator to monitor real-time SO₂ concentration during flights and thus obtain more concentrated volcanic plume samples through precise adjustment of the hovering position. We attached the improved SeIPS to a drone at Nakadake crater, Aso volcano (Japan), and successfully obtained volcanic plume samples ejected from the crater more concentrated than those obtained by using previous version of SeIPS in 2019. Additionally, we found a significant linear correlation between the reciprocal of the concentration and isotopic ratios for the ²H/¹H ratios of H₂, ¹⁸O/¹⁶O ratios of CO₂, and ¹³C/¹²C ratios of CO₂ within the plume samples. Based on the isotopic ratios of fumarolic H₂ (δ²H = -239 ± 6‰) and fumarolic CO₂ (δ¹³C = -3.58 ± 0.85‰ and δ¹⁸O = +22.01 ± 0.68‰) determined from the linear correlations, we estimated the apparent equilibrium temperatures (AETs) with magmatic H₂O simultaneously and precisely for the first time in erupting volcanoes, assuming hydrogen isotope exchange equilibrium between H₂ and H₂O (AET_D = 629 ± 32°C) and oxygen isotope exchange equilibrium between CO₂ and H₂O (AET_{18O} = 266 ± 65°C). We found that the AET_{18O} was significantly lower than the AET_D in the crater. While the temperature of the magmatic gases was originally 600°C or more, most of the gases cooled just beneath the crater to temperatures around the boiling point of water. The improved SeIPS enable us to determine both AET_D and AET_{18O} in eruptive volcanoes, wherein fumaroles are inaccessible. Simultaneous and precise determination of both the AET_{18O} and AET_D can provide novel information on each volcano, such as the physicochemical conditions of magma degassing and the development of fluid circulation systems beneath each volcano.

Keywords: SeIPS, unoccupied aerial systems, volcanic plume, stable isotopes, molecular hydrogen, carbon dioxide, fumarole, temperature assuming isotope exchange equilibrium

INTRODUCTION

Both chemical and isotopic compositions of pure volcanic gases ejected from fumaroles (termed “fumarolic gases” in this study) have provided information on each volcano, such as the physicochemical conditions of magma degassing and the development of fluid circulation systems (e.g. Ohba et al., 1994; Taran et al., 1995; Shinohara et al., 2002; Aiuppa et al., 2007). Monitoring their temporal changes is useful for forecasting volcanic eruptions (e.g. Ohsaka et al., 1980; Kagoshima et al., 2016; Stix and de Moor, 2018; Ohba et al., 2019; Ohba et al., 2021). Direct sampling of fumarolic gases, however, is neither practical nor safe for many active volcanoes in the world.

Nevertheless, we can estimate the major chemical composition of fumarolic gases remotely (i.e., a safe distance from the fumaroles), through the precise determination of the chemical composition of diluted fumarolic gases in the air (termed “volcanic plumes” in this study), using techniques such as spectroscopy (e.g. Stoiber and Jepsen, 1973; Mori et al., 1993; Francis et al., 1998), in-plume gas analysis using a portable multi-sensor system (e.g. Aiuppa et al., 2005; Shinohara, 2005), and in-plume gas sampling using unoccupied aircraft systems (UAS) (e.g. Hirabayashi et al., 1982; James et al., 2020). In addition to the chemical compositions, we can remotely estimate the stable isotopic compositions of fumarolic gases through the precise determination of both chemical and isotopic compositions in volcanic plumes. Based on the concentrations and $^2\text{H}/^1\text{H}$ ratios of molecular hydrogen (H_2) in volcanic plumes, the $^2\text{H}/^1\text{H}$ ratios of fumarolic H_2 ejected from inaccessible fumaroles can be estimated remotely by subtracting the contribution of atmospheric H_2 in the plumes (Tsunogai et al., 2011; Tsunogai et al., 2013; Tsunogai et al., 2016). Based on the observations of both the concentration and isotopic ratios ($^{13}\text{C}/^{12}\text{C}$ ratios and/or $^{18}\text{O}/^{16}\text{O}$ ratios) of carbon dioxide (CO_2) in volcanic plumes, those of fumarolic CO_2 can also be estimated remotely by subtracting the contribution of atmospheric CO_2 in volcanic plumes (Chiodini et al., 2010; Rizzo et al., 2014; Fischer and Lopez, 2016; Schipper et al., 2017; Shingubara et al., 2021). Both $^2\text{H}/^1\text{H}$ and $^{18}\text{O}/^{16}\text{O}$ ratios of fumarolic H_2 and fumarolic CO_2 , respectively, can be used to estimate the temperature of fumaroles (Mizutani, 1983; Chiodini et al., 2000; Tsunogai et al., 2011; Schipper et al., 2017; Shingubara et al., 2021). The $^{13}\text{C}/^{12}\text{C}$ ratio of fumarolic CO_2 can be used to clarify the carbon source of magma and/or the degree of magma degassing in each volcano (Gerlach and Taylor, 1990; Sano and Marty, 1995; Chiodini et al., 2010). Consequently, we can remotely detect physical changes in magmatic and/or hydrothermal activities in each volcano, based on the temporal changes in the isotopic ratios of fumarolic H_2 and CO_2 (Mizutani, 1983; Chiodini et al., 2000; Tsunogai et al., 2011; Tsunogai et al., 2016).

Determination of the isotopic ratios of fumarolic CO_2 in volcanic plumes, however, has been difficult in many inaccessible fumaroles in the world, owing to the elevated concentration of CO_2 in tropospheric air. While H_2 shows a concentration of 0.5 ppm in background tropospheric air, CO_2 may show a concentration of more than 400 ppm. Additionally, more enrichment can be observed in the tropospheric air close to

urban areas (Shinohara et al., 2020). Thus, highly concentrated volcanic plume samples are required to successfully subtract the contribution of atmospheric CO_2 in volcanic plumes (Fischer and Lopez, 2016; Shinohara et al., 2020; Shingubara et al., 2021).

Recently, we developed an automatic volcanic plume sampler named SelPS (SO_2 Selective Plume Sampler), wherein an output signal from a sulfur dioxide (SO_2) sensor triggered a pump to collect samples when the SO_2 concentration exceeded a predefined threshold (Shingubara et al., 2021). Additionally, we attached the SelPS to a drone (UAS) and obtained samples of volcanic plumes ejected from the summit crater of the Nakadake central cone (Nakadake crater) of Aso volcano, Japan. The samples showed higher concentrations of H_2 and CO_2 than those acquired manually in flasks at the crater rim (Shingubara et al., 2021). We also determined the precise $^2\text{H}/^1\text{H}$ ratio of fumarolic H_2 in the volcano by subtracting the atmospheric contribution from the samples. Conversely, the isotopic compositions ($^{13}\text{C}/^{12}\text{C}$ and $^{18}\text{O}/^{16}\text{O}$ ratios) of fumarolic CO_2 estimated by subtracting the atmospheric contribution from the samples have insufficient precision for detailed discussions using the values (Shingubara et al., 2021). While the $^{13}\text{C}/^{12}\text{C}$ ratios of high temperature ($>100^\circ\text{C}$) fumarolic CO_2 in subduction zone volcanoes showed a narrow variation from -8.5 to -2.0‰ in the $\delta^{13}\text{C}$ scale (the definition of $\delta^{13}\text{C}$ is presented in *Analysis and Data Processing*) (Sano and Marty, 1995; Symonds et al., 2003), the $\delta^{13}\text{C}$ value of fumarolic CO_2 in the Nakadake crater, estimated by subtracting the atmospheric contribution, was accompanied by an uncertainty of more than 10‰ (Shingubara et al., 2021), making it difficult to discuss the $\delta^{13}\text{C}$ value. The $\delta^{13}\text{C}$ value of fumarolic CO_2 in Manam (Papua New Guinea) determined from the volcanic plume samples collected through a drone-borne sampler using a timer-triggered pump was also accompanied by an uncertainty too large to discuss the $\delta^{13}\text{C}$ value (Liu et al., 2020). While the $^{18}\text{O}/^{16}\text{O}$ ratio of fumarolic CO_2 in the Nakadake crater estimated by subtracting the atmospheric contribution from the samples was more precise (showing $+16.7 \pm 6.6\text{‰}$ in the $\delta^{18}\text{O}$ scale; the definition of $\delta^{18}\text{O}$ is presented in *Analysis and Data Processing*), the $\delta^{18}\text{O}$ value of fumarolic CO_2 has insufficient precision to reliably estimate the outlet temperature of fumaroles (Shingubara et al., 2021). During the observation in Nakadake crater, the maximum concentration of CO_2 was 531 ppm while the background concentration of CO_2 was 470 ppm (Shingubara et al., 2021), so that the maximum mole fraction (Sasakawa et al., 2008; Tsunogai et al., 2011) of fumarolic CO_2 within the total CO_2 in the plume was 11%. During the observation in Manam, the maximum concentration of CO_2 was 494 ppm while the background concentration of CO_2 was 409 ppm, so that the maximum mole fraction of fumarolic CO_2 within the total CO_2 in the plume was 21% (Liu et al., 2020). Thus, more concentrated volcanic plume samples are required to subtract the contribution of atmospheric gases in volcanic plumes and to precisely determine the isotopic ratios of fumarolic CO_2 .

In this study, we added a radio transmission function to SelPS, which enabled our drone operator to monitor SO_2 concentration determined by SelPS during flights, and thus obtain more concentrated volcanic plume samples through precise

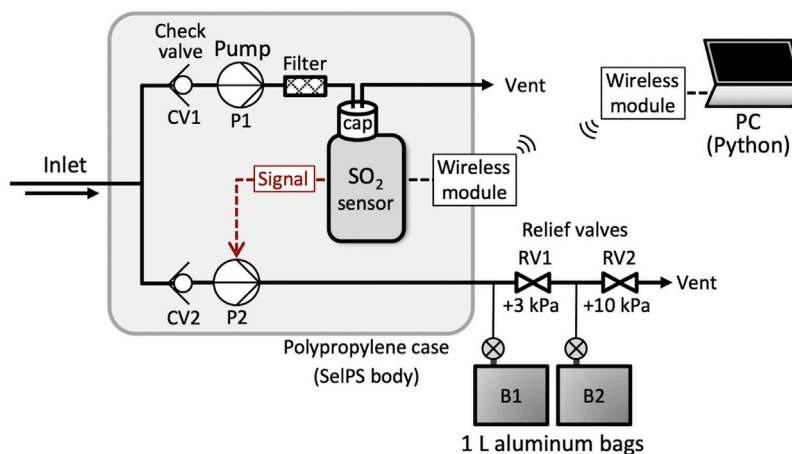


FIGURE 1 | The internal flow diagram of the plume sampler SelPS (modified from Shingubara et al., 2021). Gas samples drawn in at the gas inlet were partitioned into two lines in parallel, each of which was connected to a diaphragm pump (DPO125, Nitto Kohki Co., Ltd., Japan). Pump P1, running continuously throughout a flight, introduced gas at a flow rate of approximately 0.5 L/min to a filter (ZFC33, SMC Corp., Japan) and subsequently to an electrochemical SO₂ sensor (ToxiRAE Pro EC PGM-1860, RAE Systems Inc., United States), which continuously measured SO₂ concentrations. A wireless module was newly added to monitor the real-time SO₂ concentration during flights and thus obtain more concentrated volcanic plume samples through the precise adjustment of the hovering position.

adjustment of the hovering position of the drone. We also raised the predefined threshold of the SO₂ sensor, which triggered a pump to collect the samples. In this paper, we report the revisions made to the SelPS, along with the results of sampling volcanic plume samples in the same Nakadake crater (Aso volcano) using the revised SelPS in 2020.

MATERIALS AND METHODS

Automatic Plume Sampler SelPS

The basic structure of SelPS was the same as that reported in a previous study (Figure 1) (Shingubara et al., 2021). The sampler weighed 1.3 kg in total and was housed inside a polypropylene case (23.0 cm length × 17.0 cm width × 7.5 cm height). Plume/air samples drawn into the sampler were partitioned into two parallel lines, each connected to a diaphragm pump (Figure 1). The P1 pump, running continuously throughout each flight, introduced gas at a flow rate of approximately 0.5 L/min to an electrochemical SO₂ sensor (ToxiRAE Pro, RAE Systems Inc., United States), which continuously measured the SO₂ concentration. The SO₂ concentrations from 0 to 19.9 ppm were recorded at 1 s intervals in a memory at 0.1 ppm resolution. Additionally, the analog output signal from the SO₂ sensor (0–1.5 V, which corresponds to SO₂ concentrations from 0 to 155 ppm) was converted to a 10 bit digital format and continuously sent to the operator at the ground during each flight through a commercial wireless module using a 920 MHz band for the communication.

As reported previously by Shingubara et al. (2021), the output signal for the vibration alarm function equipped with the SO₂ sensor was applied to trigger the sampling. When the SO₂ concentration exceeded a predefined threshold, the output signal turned the P2 pump (flow rate = 2 L/min) on, such that

the SO₂-enriched gas samples were introduced into two 1 L aluminum bags (B1 and B2) connected through a relief valve (cracking pressure = +3 kPa; Figure 1) to individually fill the bags (Shingubara et al., 2021). When the first aluminum bag (B1) became full, the relief valve opened to introduce the SO₂-enriched gas eluted from P2 into the second bag (B2). When the second aluminum bag (B2) also became full, another relief valve (cracking pressure = +10 kPa) attached at the downstream end of the second bag opened to vent the additional SO₂-enriched gas eluted from P2 into the air (Figure 1) (Shingubara et al., 2021).

Sampling

Aso Volcano is a Quaternary caldera volcano located in central Kyushu, Japan (Supplementary Figure S1). Gigantic eruptions with pyroclastic flow starting from the Pleistocene formed both the Aso caldera (25 km from north-south and 18 km from east-west) and the central cones, among which the Nakadake crater (the first crater of Nakadake central cone) is currently the most active. In this crater, volcanic plumes were continuously ejected from the inaccessible fumaroles at the bottom. The fumaroles in this crater have been classified into two: the central vent of the crater (main vent) and the fumaroles on the southern wall (southern fumaroles) for the last 20 years (Figure 2) (Shinohara et al., 2018). Both vents ejected white plumes during sampling. The most recent explosive, strombolian eruptions from this crater prior to the present sampling period started in November 2014 and ended in May 2015 (Shinohara et al., 2018; Tsunematsu et al., 2019; Yokoo et al., 2019).

Plume sampling using drones in this study was conducted on 20 October 2020 (Supplementary Figure S2). The drone used for the sampling was the same as that used in a previous study (Shingubara et al., 2021); a battery-powered octo-rotor multicopter (Spreading Wings S1000, DJI, China) with a GPS module that recorded the latitude, longitude, and altitude at

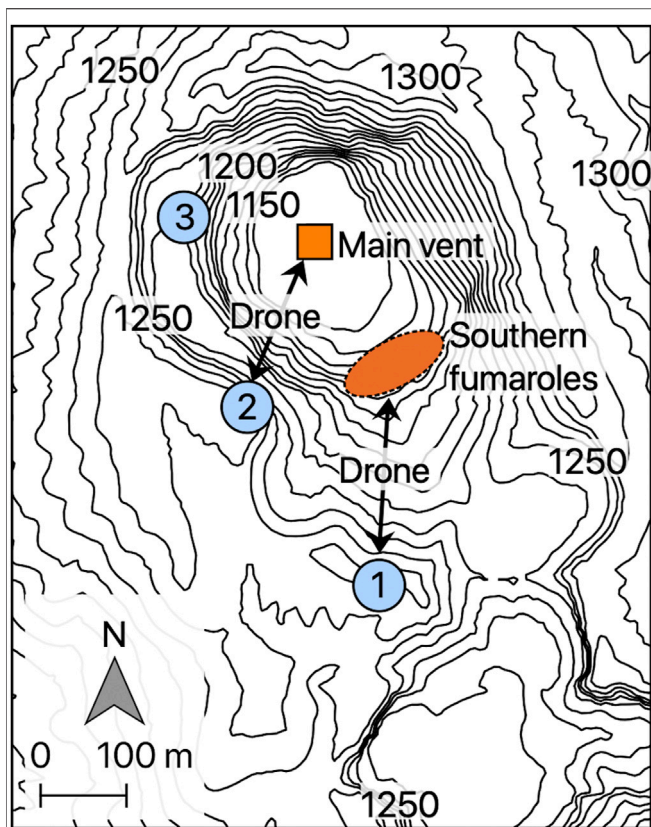


FIGURE 2 | The topographic map of the Nakadake crater, Aso volcano, along with the locations of the large vent at the central part of the crater (main vent) and the active fumarolic area on the southern wall of the crater (southern fumaroles; base map from Geospatial Authority of Japan). The drone with SelPS was operated from an observation deck at the southern rim of the crater (the blue circle numbered 1) during the first four flights and from an observation deck at the south-western rim of the summit crater (the blue circle numbered 2) during the subsequent three flights. The location of the western rim of the summit crater where plume samples were collected manually into pre-evacuated flasks are shown by the blue circle numbered 3.

200 Hz. The maximum payload weight was 3.1 kg. We fixed our plume sampler SelPS at the foot of the landing gear, approximately 30 cm beneath the multicopter (**Figure 3**). The entire sampler, including the aluminum bags, was covered with a plastic net during the flights to prevent any interaction with the rotors. The inlet tube made of Tygon tubing (4 mm inner diameter, 6 mm outer diameter, and 3.0 m in length) was allowed to hang down from the multicopter during the flights (**Figure 3**) to obtain the plume sample from its upper side, without our multicopter getting deep into the plume.

Our target was the plume ejected from the southern fumaroles during the first four flights; and it was subsequently changed to the plume ejected from the main vent during the last three flights (**Figure 2**). In accordance with the change in the target, we also changed the operation deck (departure/arrival point) on the crater rim from sites 1 to 2 (**Figure 2**). During each flight, the drone hovered over the plumes for several minutes. The threshold SO_2 concentration of SelPS during the sampling was set at

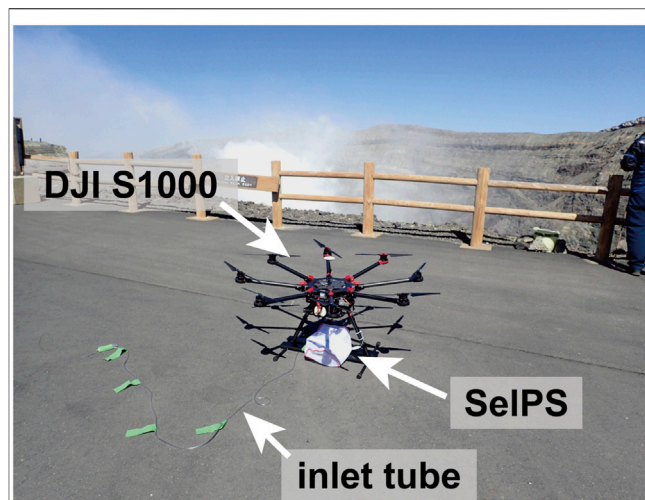


FIGURE 3 | A photo of the plume sampler SelPS fixed on the DJI S1000 drone at Aso volcano. The sampler and aluminum bags are covered with a white plastic net.

19.9 ppm throughout the flights, while it was set at 1.0 or 5.0 ppm during the samplings in 2019.

During the flight, our personal computer (PC) at the operation deck continuously received the wireless signal of the SO_2 sensor transmitted from the SelPS. Based on the automatic conversion of the concentration to decimal values on the PC, our operator could monitor real-time SO_2 concentrations during flights. Thus, more concentrated volcanic plume samples could be obtained by precisely adjusting the position of the drone hovering over the plumes. Moreover, our operator could decide the timing for the drone to stop sampling from the monitored SO_2 concentration, based on the total integrated time when the SO_2 concentration exceeded the gas sampling threshold (19.9 ppm in this study). As it took approximately 35 s to fill up one bag, 70 s was a sufficient total integrated time to fully fill up the bags in each flight.

After each flight, the aluminum bags filled with plume samples were replaced with empty bags on the operation deck. The batteries of the drone were replaced and it subsequently moved to the next flight. The plume samples collected in the aluminum bags were transferred to pre-evacuated 500 ml glass flasks with stopcocks using Viton O-rings for sealing (Tsunogai et al., 2003; Tsunogai et al., 2011), a few hours after sampling (Shingubara et al., 2021).

In addition to the samples taken by using SelPS on a drone, plume samples occasionally transported to the crater rim by the wind were also manually collected into pre-evacuated 1 L glass flasks with a stopcock (Tsunogai et al., 2011) at site 3 in **Figure 2** on October 19 and 20, 2020 ($n = 13$; **Table 1**). While it was difficult to focus the plume target in the case of manual sampling, most plumes sampled were apparently derived from the main vent. Furthermore, a background air sample was manually collected into a flask in a similar manner at the upwind side of the crater rim (**Table 1**) to determine concentrations and

TABLE 1 | List of samples analyzed in this study, along with the concentration of SO₂, concentration and isotopic compositions of H₂, and concentration and isotopic compositions of CO₂ in the samples.

ID	Date	Time	Type ^a	Target ^b	[SO ₂] ^c (ppm)	[H ₂] (ppm)	1,000 δ ² H	[CO ₂] (ppm)	1,000 δ ¹³ C	1,000 δ ¹⁸ O
D01	2020/10/20	11:10	F01	SF	30.7	0.95	-24.5 ± 5.6	445	-9.7	+40.8
D02	2020/10/20	11:10	F01	SF	30.7	0.96	-48.2 ± 6.2	437	-10.1	+40.9
D04	2020/10/20	11:20	F02	SF	31.6	0.92	-32.3 ± 5.7	445	-9.9	+40.7
D05	2020/10/20	11:40	F03	SF	36.8	1.01	-56.7 ± 5.3	456	-10.1	+40.1
D06	2020/10/20	11:40	F03	SF	36.8	1.03	-67.4 ± 4.9	445	-9.5	+40.0
D07	2020/10/20	11:50	F04	SF	30.3	0.95	-34.4 ± 5.5	425	-10.6	+40.9
D08	2020/10/20	11:50	F04	SF	30.3	0.97	-41.0 ± 5.3	426	-9.6	+40.7
D09	2020/10/20	12:40	F05	MV	27.8	1.19	-70.4 ± 4.5	456	-9.7	+39.4
D10	2020/10/20	12:40	F05	MV	27.8	1.30	-95.4 ± 4.4	452	-9.9	+39.7
D11	2020/10/20	12:50	F06	MV	50.1	2.09	-144.8 ± 3.0	514	-9.4	+37.6
D12	2020/10/20	12:50	F06	MV	50.1	1.89	-125.2 ± 3.2	501	-9.3	+37.8
D13	2020/10/20	13:00	F07	MV	40.0	1.15	-92.2 ± 4.1	470	-9.1	+39.1
D14	2020/10/20	13:00	F07	MV	40.0	1.33	-104.8 ± 3.8	498	-9.2	+38.4
M01	2020/10/19	14:01	manual	MV	6.0	0.71	+27.1 ± 6.0	443	-9.8	+40.8
M02	2020/10/19	14:04	manual	MV	7.0	0.57	+90.0 ± 7.2	413	-10.1	+41.6
M03	2020/10/19	14:09	manual	MV	10.4	0.75	+29.0 ± 6.0	428	-10.1	+40.9
M04	2020/10/19	14:10	manual	MV	13.6	0.86	-13.6 ± 5.3	439	-9.7	+40.4
M05	2020/10/19	14:14	manual	MV	9.3	0.74	+25.9 ± 5.8	423	-9.9	+40.8
M06	2020/10/19	14:23	manual	MV	10.6	1.07	-56.4 ± 4.3	453	-9.4	+39.7
M07	2020/10/19	14:24	manual	MV	8.1	0.73	+20.9 ± 5.7	432	-9.9	+41.1
M08	2020/10/19	14:35	manual	MV	8.2	0.84	-6.8 ± 5.4	446	-9.8	+40.4
M09	2020/10/19	14:44	manual	MV	11.5	1.19	-84.4 ± 4.0	454	-9.9	+39.2
M10	2020/10/19	14:54	manual	MV	7.8	0.75	+11.3 ± 5.9	438	-10.1	+40.8
M11	2020/10/19	14:58	manual	MV	19.9	0.89	-35.8 ± 5.1	437	-10.2	+40.7
M12	2020/10/19	15:01	manual	Air	0.0	0.62	+80.4 ± 7.0	416	-10.0	+41.3
M14	2020/10/20	12:27	manual	MV	>19.9	0.87	-10.6 ± 5.0	444	-10.0	+40.3
M15	2020/10/20	12:30	manual	MV	>19.9	0.71	+34.6 ± 6.0	435	-9.8	+41.1

^aThe "manual" tags denote samples collected manually at the crater rim, while the flight number (number with prefix "F") denotes those collected automatically using SelPS.

^bThe target of each sampling; SF, is the plume derived from the fumaroles on the southern wall of the crater and MV, is that derived from the main vent in the crater. Air is the background air collected at the upwind side of the crater.

^cThe average SO₂ concentration during sampling (i.e., during the first 70 s in total when [SO₂] exceeded 19.9 ppm) for the samples collected by SelPS, and the SO₂ concentration at the start of sampling for the samples collected manually.

isotopic ratios of CO₂ and H₂ in background air during sampling, because their values are not always the same in troposphere (Price et al., 2007; Welp et al., 2011).

Analysis and Data Processing

The components analyzed in this study, along with the analytical methods and data processing, were the same as those in a previous study (Shingubara et al., 2021). The brief explanation is as follows.

The concentrations and ²H/¹H ratios of H₂ in the plume/air samples collected were determined using a continuous-flow isotope ratio mass spectrometer (CF/IRMS) system at Nagoya University, wherein Delta V Advantage (Thermo Fisher Scientific) was used for the mass spectrometer (Komatsu et al., 2011; Tsunogai et al., 2020). The concentrations, ¹⁸O/¹⁶O ratios, and ¹³C/¹²C ratios of CO₂ in the samples were analyzed by another CF/IRMS system at Nagoya University, wherein Finnigan MAT 252 (Thermo Fisher Scientific) was used for the mass spectrometer (Ijiri et al., 2003; Kawagucci et al., 2005). In this study, all isotope ratios are expressed in terms of delta (δ), defined by the following equation:

$$\delta^m X = \frac{R_{\text{sample}}}{R_{\text{standard}}} - 1$$

where ^mX denotes the heavier isotope (²H, ¹⁸O, or ¹³C) and R_{sample} and R_{standard} represent the abundance ratios of the heavier isotope to the lighter isotope (²H/¹H, ¹⁸O/¹⁶O, or ¹³C/¹²C) in the sample and standard, respectively. The δ²H and δ¹⁸O values are expressed relative to the Vienna Standard Mean Ocean Water (VSMOW) standard, and the δ¹³C values are expressed relative to the Vienna Pee Dee Belemnite (VPDB) standard.

The analytical precision to determine the H₂ concentration was ±3% and that to determine δ²H of H₂ was ±3.0–7.2‰ in our study, depending on the quantity of H₂ introduced into the CF/IRMS system (Komatsu et al., 2011). The analytical precision to determine CO₂ was ±3% for its concentration and ±0.3‰ for both δ¹⁸O and δ¹³C.

For the δ value of the fumarolic H₂ (or CO₂), we adopted the intercept of the regression line between the δ values and the reciprocals of concentrations (Keeling, 1958; Tsunogai et al., 2011; Fischer and Lopez, 2016; Shingubara et al., 2021) using the weighted least squares approach (York, 1969; Tsunogai et al., 2011). In this approach, the differences in the magnitude of errors among individual data were considered (Cantrell, 2008; Tsunogai et al., 2011).

Based on the estimated δ²H value of fumarolic H₂, we can estimate the apparent equilibrium temperature for δ²H using the following equation:

$$\text{AET}_D = \{4.474 \times 10^{-12} \times \Delta_D^2 + 3.482 \times 10^{-9} \times \Delta_D + 9.007 \times 10^{-8}\}^{-1/2} - 273.15$$

where AET_D denotes the apparent temperature (in degrees Celsius) assuming hydrogen isotope exchange equilibrium between fumarolic H_2 and fumarolic H_2O , and Δ_D represents $10^3 \ln(\alpha_{\text{H}_2\text{O}-\text{H}_2})$, where $\alpha_{\text{H}_2\text{O}-\text{H}_2}$ represents the apparent fractionation of hydrogen isotopes between H_2O and H_2 [$\alpha_{\text{H}_2\text{O}-\text{H}_2} = (\delta^2\text{H}(\text{H}_2\text{O}) + 1)/(\delta^2\text{H}(\text{H}_2) + 1)$]. This equation was used by Tsunogai et al. (2011), and was obtained from the equilibrium fractionation factor reported by Richet et al. (1977).

Based on the estimated $\delta^{18}\text{O}$ value of fumarolic CO_2 , we can estimate the apparent equilibrium temperature for $\delta^{18}\text{O}$ using the following equation:

$$10^3(\alpha_{\text{CO}_2-\text{H}_2\text{O}}) = -5.7232 + 20.303 \times 10^3 / (\text{AET}_{180}) - 11.977 \times 10^6 / (\text{AET}_{180})^2 + 3.7432 \times 10^9 / (\text{AET}_{180})^3$$

where AET_{180} denotes the apparent temperature (in Kelvin in this equation, but in degrees Celsius in the text), assuming oxygen isotope exchange equilibrium between fumarolic CO_2 and fumarolic H_2O , and $\alpha_{\text{CO}_2-\text{H}_2\text{O}}$ represents the apparent fractionation of oxygen isotopes between fumarolic CO_2 and fumarolic H_2O [$\alpha_{\text{CO}_2-\text{H}_2\text{O}} = (\delta^{18}\text{O}(\text{CO}_2) + 1)/(\delta^{18}\text{O}(\text{H}_2\text{O}) + 1)$]. This equation is empirical and obtained from the observation of Italian volcanoes (Chiodini et al., 2000). The expressions and units in the original literature were used to calculate the AETs.

Assuming that H_2 and H_2O (or CO_2 and H_2O) are under the hydrogen isotope exchange equilibrium (or oxygen isotope exchange equilibrium) in a fumarole, the estimated AET_D (or AET_{180}) corresponds to the outlet temperature of the fumarole. For the hydrogen and oxygen isotopic compositions of magmatic H_2O in the Nakadake crater, the average δ values of the magmatic H_2O in convergent-plate volcanoes, estimated by Tsunogai et al. (2011) for $\delta^2\text{H}$ and by Sambuichi et al. (2021) for $\delta^{18}\text{O}$, were used ($\delta^2\text{H} = -24.5 \pm 7.3\text{‰}$, $\delta^{18}\text{O} = +6.0 \pm 3.0\text{‰}$).

RESULTS

While we took 14 plume samples in total through seven drone flights, one of the aluminum bags leaked during storage until it was transferred into a glass bottle. Consequently, 13 plume samples were transferred into glass bottles and analyzed for both concentrations and isotopic compositions (Table 1). Within the 13 plume samples, the initial seven samples were collected at the plume ejected from the southern fumaroles, while the rest were collected at that ejected from the main vent.

The temporal variation in the SO_2 concentration recorded in the internal memory of SelPS during the flights is shown by the blue line in Figure 4 (denoted as “internal”), along with the SO_2 concentration transmitted to the operator through a wireless module and recorded on the PC at the operation deck (shown by the orange line, denoted as “wireless” in the same figure). While the upper concentration limit that could be recorded on the internal memory was 19.9 ppm, the upper concentration limit that was originally determined on the same

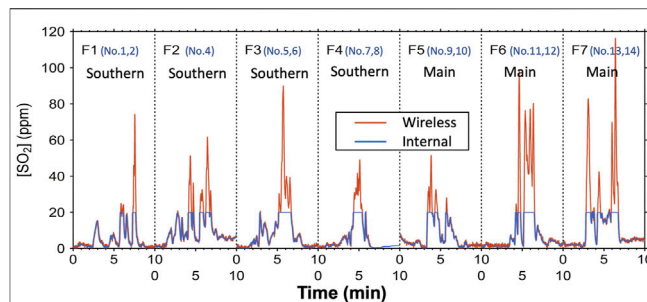


FIGURE 4 | Temporal variations in the SO_2 concentration of the gas drawn into SelPS at Aso volcano recorded in the internal memory (blue line), along with that sent to the operator through the wireless module of SelPS and recorded on the PC (orange line). Labels F1-F7 denote the individual flights. The duration when the SO_2 concentration recorded on the PC (shown by the orange line) was higher than that recorded on the internal memory of SelPS (the blue line) corresponds to the SO_2 signal turned P2 on for sampling (see text for the details).

sensor but sent to the PC at the operation deck through the wireless module was much higher than this threshold (more than 150 ppm). Additionally, the upper concentration limit that could be recorded on the internal memory corresponded with the gas sampling threshold set for the sampling. Consequently, the duration when the SO_2 concentration recorded on the PC (the orange line in Figure 4) was higher than that recorded in the internal memory of SelPS (the blue line in the same figure) corresponded to the duration of sampling. As it takes approximately 35 s to fill up one bag, the first 70 s of the integrated time when the orange line was higher than the blue line in Figure 4 corresponded to the time of sampling. The relationship between the concentrations of SO_2 and CO_2 in the plume/air samples collected automatically by SelPS (orange circles: plume samples derived from the main vent; blue squares: those derived from the southern fumaroles) are shown in Figure 5A, along with those taken manually into pre-evacuated flasks (white circles). While we connected the aluminum bags through a relief valve (+3 kPa) to individually fill the bags, we found that the samples in the bags mixed with each other to some extent during sampling probably because the first relief valve often cracked under the pressure much lower than the setting value (+3 kPa) in the air where the atmospheric pressure was much lower than that on the ground. Consequently, we used each average SO_2 concentration during the sampling of each flight (i.e., during the first 70 s of the integrated time exceeding the sampling threshold concentration) for the SO_2 concentration of the samples collected by SelPS during each flight (Table 1). Please note that the error in the determined SO_2 concentration was around 10% or more because it was difficult to determine the exact time of sampling during each flight.

DISCUSSION

Origin of Excess CO_2 and H_2 in the Plume

As clearly presented in Figure 5A showing the relation between the concentrations of SO_2 and CO_2 , all the plume samples obtained during SO_2 enrichment were also enriched in CO_2 ;

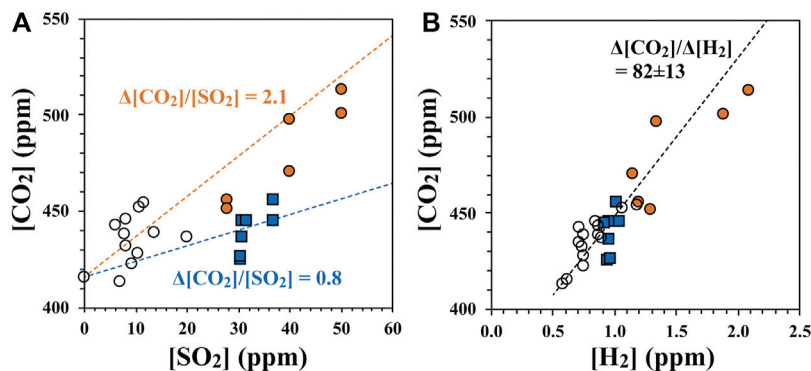


FIGURE 5 | (A) Relationship between the concentrations of SO_2 and CO_2 and **(B)** that between the concentrations of H_2 and CO_2 in the plume/air samples collected automatically by SelPS (orange circles: plume samples derived from the main vent; blue squares: those derived from the southern fumaroles), as well as those derived from the main vent and collected manually into pre-evacuated flasks (white circles) at the Nakadake crater, Aso volcano. The orange dotted line in **(A)** represents the regression line calculated for those derived from the main vent and the background air sample. The blue dotted line in **(A)** represents the regression line calculated for those derived from the southern fumaroles and the background air sample. The black dotted line in **(B)** represents the regression line calculated for all the plume/air samples. All the regression lines were calculated according to Cantrell, (2008). The $\Delta[\text{CO}_2]$ (or $\Delta[\text{H}_2]$) values in the figures denote excess CO_2 (or H_2) from CO_2 (or H_2) in the background air.

the $\Delta[\text{CO}_2]/[\text{SO}_2]$ ratios were approximately 2.1 and 0.8 for the main vent and southern fumaroles, respectively, where $\Delta[\text{CO}_2]$ denoted excess CO_2 from CO_2 in the background air. While the average $\Delta[\text{CO}_2]/[\text{SO}_2]$ ratio in the main vent was higher than that in the southern fumaroles during our sampling, the differences between the slopes were statistically insignificant.

Using a portable multi-sensor system, Shinohara et al. (2018) determined the spatial and temporal variations in the concentrations of major components in the volcanic plume ejected from the Nakadake crater. Their estimated $\Delta[\text{CO}_2]/[\text{SO}_2]$ ratios ranged from 0.35 to 10 during the observation period from October 2003 to May 2015. The $\Delta[\text{CO}_2]/[\text{SO}_2]$ ratios obtained in this study agree well with previous observations. We concluded that both excess CO_2 and SO_2 in the plume samples were ejected from the fumaroles in the Nakadake crater. In contrast to CO_2 in the volcanic plume of Sakurajima volcano (Shinohara et al., 2020), variations in the mole fractions of fumarolic gases within the tropospheric air were responsible for those in CO_2 concentrations in the plume samples.

The relationships between the concentrations of H_2 and CO_2 in the plume/air samples collected automatically by SelPS are shown in **Figure 5B**, along with those collected manually into pre-evacuated flasks. As shown in the figure, all the plume samples obtained during CO_2 enrichment were also enriched in H_2 . The $\Delta[\text{CO}_2]/\Delta[\text{H}_2]$ ratios were 82 ± 14 , which corresponded to $\Delta[\text{H}_2]/\Delta[\text{CO}_2]$ ratios of 0.0126 ± 0.022 . Additionally, in contrast to the $\Delta[\text{CO}_2]/[\text{SO}_2]$ ratios, the $\Delta[\text{CO}_2]/\Delta[\text{H}_2]$ ratios were homogeneous, irrespective to the fumaroles from which the plumes derived (main vent or southern fumaroles).

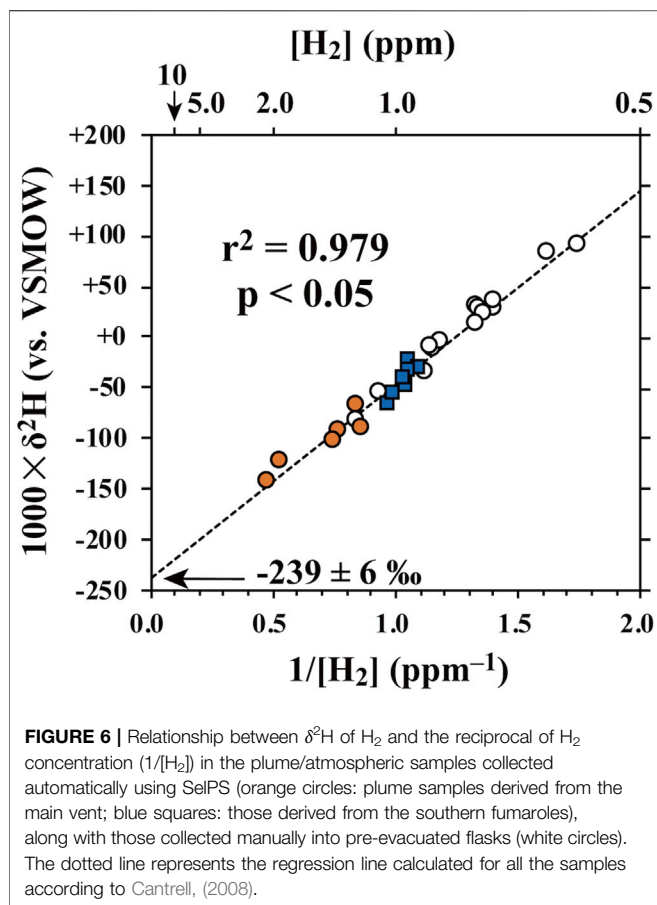
Shinohara et al. (2018) also reported large temporal variations in the $\Delta[\text{H}_2]/\Delta[\text{CO}_2]$ ratios of the volcanic plume ejected from the Nakadake crater, from 0.006 to 0.38. While the $\Delta[\text{H}_2]/\Delta[\text{CO}_2]$ ratios determined in this study corresponded to one of the

lowermost $\Delta[\text{H}_2]/\Delta[\text{CO}_2]$ ratios for the plume ejected from the crater, all the $\Delta[\text{H}_2]/\Delta[\text{CO}_2]$ ratios were less than 0.015 during their observations after March 2015 (Shinohara et al., 2018). We concluded that the obtained $\Delta[\text{H}_2]/\Delta[\text{CO}_2]$ ratios were similar to those of the plume ejected from the crater. In addition to the excess CO_2 in the plume samples, we concluded that the excess H_2 in the plume was derived from the fumaroles in the crater. Moreover, the variations in the mole fractions of fumarolic gases within the background air were responsible for the various H_2 concentrations in the plume samples shown in **Figure 5B**.

Comparison With the Samples Collected Manually and Those Collected by Using Old SelPS

The maximum concentration of CO_2 within the samples obtained by SelPS (514 ppm; **Figure 5A**) was considerably higher than that collected manually in flasks at the crater rim (454 ppm; **Figure 5A**). The maximum concentration of H_2 within the samples obtained by SelPS (2.1 ppm; **Figure 5B**) was also higher than that collected manually in flasks at the crater rim (1.2 ppm; **Figure 5B**). The same results were obtained for $[\text{SO}_2]$ (**Table 1** and **Figure 5A**). We concluded that the drone-borne sampler SelPS had the advantage of collecting more concentrated (i.e., less diluted) plume samples than those collected manually at the crater rim.

Additionally, we succeeded in collecting more concentrated (i.e., less diluted) plume samples in 2020 compared to those obtained in 2019 using previous version of SelPS. While the background $[\text{CO}_2]$ was 470 ppm in 2019, the maximum $[\text{CO}_2]$ was 531 ppm, such that the difference between the maximum and background $[\text{CO}_2]$ ($\Delta[\text{CO}_2]$) was 61 ppm (Shingubara et al., 2021). Thus, the maximum mole fraction (Sasakawa et al., 2008; Tsunogai et al., 2011) of fumarolic CO_2 within the total CO_2 in the plume was 11% in 2019. Conversely, while the



background $[\text{CO}_2]$ was 416 ppm, the maximum $[\text{CO}_2]$ was 514 ppm (Figure 5A); therefore, the $\Delta[\text{CO}_2]$ was 98 ppm; thus, the maximum mole fraction of fumarolic CO_2 within the total CO_2 in the plume was 19% in 2020. Furthermore, the maximum H_2 concentration in the samples obtained in this study using SelPS was higher than that in the samples obtained in 2019 using previous version of SelPS (1.8 ppm). The same results were obtained for $[\text{SO}_2]$. Although the concentrations of H_2 , CO_2 , and SO_2 in the plume could be temporally variable, the present results imply that adding a radio transmission function to the sampler was effective in collecting more concentrated plume samples, through precise adjustment of the hovering position by monitoring the real-time SO_2 concentration during flights.

The $^2\text{H}/^1\text{H}$ Ratio of Fumarolic H_2

The relationship between the $\delta^2\text{H}$ of H_2 and the reciprocal of H_2 concentration ($1/[\text{H}_2]$) in the plume/air samples collected automatically by SelPS (orange circles denote the targeted main vent, and blue squares denote the targeted southern fumaroles) at the crater is shown in Figure 6, along with those collected manually in flasks on the crater rim (white circles). The $\delta^2\text{H}$ values of H_2 in the plume samples collected automatically using SelPS (orange circles and blue squares) showed large variations, from -144.8 to -24.5‰ , while showing a linear correlation with the reciprocal of H_2

concentrations ($1/[\text{H}_2]$), irrespective of the sampling target (main vent or southern fumaroles). All the plume/air samples collected manually in flasks (open circles) were plotted on the same line as well, wherein the background air sample showing a H_2 concentration of 0.62 ppm and a $\delta^2\text{H}$ value of $+80.4 \pm 7.0\text{‰}$ (Table 1) was included. Both concentration and the $\delta^2\text{H}$ value of the background air sample compare well with that of H_2 in background tropospheric air (Price et al., 2007; Rice et al., 2010). As discussed by Tsunogai et al. (2011), the linear relationships imply that both concentrations and $\delta^2\text{H}$ values of H_2 in the samples can be explained by simple mixing between two end-members with different H_2 concentrations and different $\delta^2\text{H}$ values: fumarolic H_2 with a higher concentration and ^2H -depleted $\delta^2\text{H}$ value, and H_2 in the background air with a lower concentration and ^2H -enriched $\delta^2\text{H}$ values. Additionally, the linear relationships also implied that the $\delta^2\text{H}$ values of fumarolic H_2 were homogeneous irrespective of the sampling target (main vent or southern fumaroles), the method of sampling (automatically using SelPS or manually), and the day of sampling (October 19 or 20, 2020).

By extrapolating the linear relationship between $1/[\text{H}_2]$ and $\delta^2\text{H}$ to $1/[\text{H}_2] = 0$ to exclude the contribution of the H_2 in background air (the H_2 -depleted end-member) from the $\delta^2\text{H}$ value of each sample (Tsunogai et al., 2003), we estimated the $\delta^2\text{H}$ value of fumarolic H_2 (the H_2 -enriched end-member) to be $-239 \pm 6\text{‰}$. Thus, the AET_D was $629 \pm 32^\circ\text{C}$ (both with 1σ errors). Compared with that determined in 2019, when the $\delta^2\text{H}$ value of fumarolic H_2 was estimated to be $-134 \pm 14\text{‰}$ (Shingubara et al., 2021), the AET_D decreased by approximately 400°C . Moreover, the AET_D determined in the present study was lower than that reported for the same crater on 10 November 2010 ($868 \pm 48^\circ\text{C}$ with 1σ error; Tsunogai et al., 2011), based on the $\delta^2\text{H}$ values of plume samples collected manually into flasks. We concluded that the AET_D was temporally variable in this crater, with a variation range of more than 400°C .

Compared with the volcanic activities in August 2019, those in October 2020 were apparently less active. The maximum emission rate of SO_2 , for instance, was 1,100 tons per day in October 2020, while it was 5,200 tons per day in October 2019 (Japan Meteorological Agency, 2020). The observed decrease in AET_D at approximately 400°C is seemingly comparable to the temporal changes in volcanic activities.

The $^{13}\text{C}/^{12}\text{C}$ Ratios and $^{18}\text{O}/^{16}\text{O}$ Ratios of Fumarolic CO_2

The relationship between $\delta^{13}\text{C}$ or $\delta^{18}\text{O}$ of CO_2 and the reciprocal of CO_2 concentrations ($1/[\text{CO}_2]$) in the plume samples collected automatically by using SelPS (orange circles and blue squares) at the caldera is shown in Figures 7A,B. Those collected manually into flasks on the western crater rim are also shown in these figures. As the CO_2 concentration in the background tropospheric air (approximately 400 ppm; Tohjima, et al., 2009) was considerably higher than that of H_2 (0.5–0.6 ppm; Rice et al., 2010), the contribution of fumarolic CO_2 had been masked in the plume samples in past studies (Liu et al., 2020;

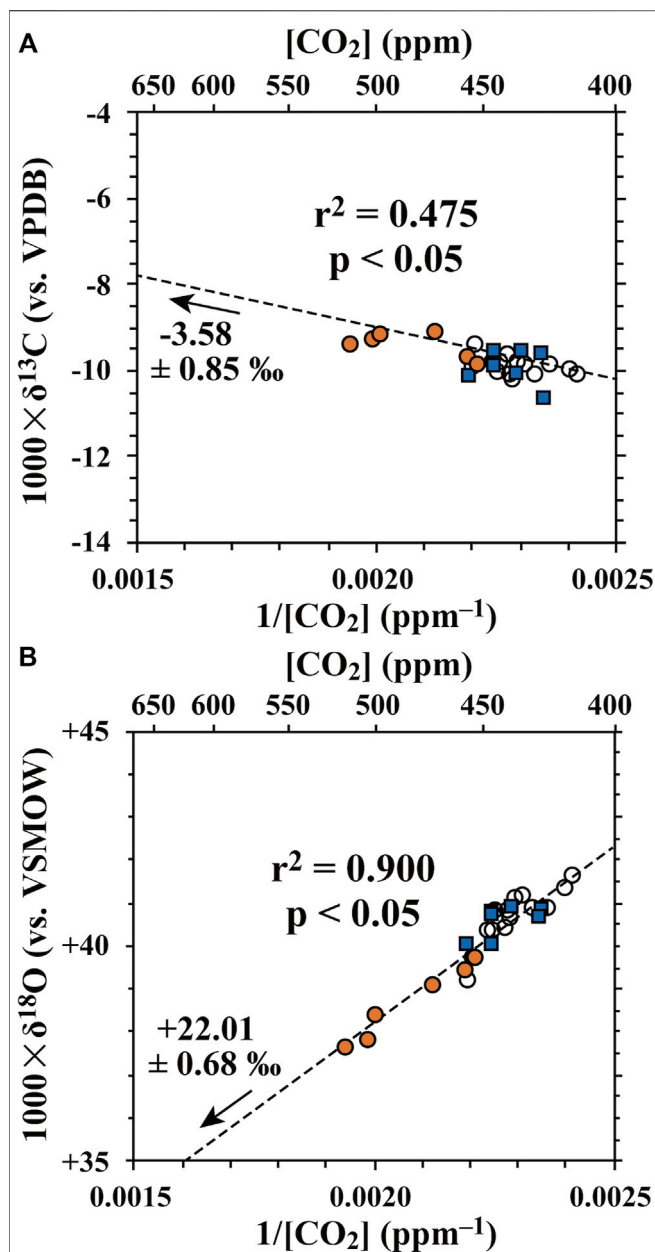


FIGURE 7 | (A) Relationships of carbon and **(B)** oxygen isotopic compositions of CO₂ with reciprocal CO₂ concentrations ($1/[\text{CO}_2]$) in the plume/air samples collected using SelPS (orange circles: plume samples derived from the main vent; blue squares: those derived from the southern fumaroles) and those collected manually into flasks (white circles). The dotted lines represent the regression lines calculated for all the samples according to Cantrell, (2008).

Shingubara et al., 2021). In addition, both $\delta^{13}\text{C}$ and $\delta^{18}\text{O}$ values of CO₂ in the background air sample (-10.0‰ and $+41.3\text{‰}$; **Table 1**) showing slight deviations from those of CO₂ in tropospheric background air (Welp et al., 2011; Peters et al., 2018) implied that the background air sample taken at upwind side of the crater rim had been influenced by the interactions with the sources/sinks of tropospheric CO₂ around the crater.

However, we found a significant linear correlation between the reciprocal of CO₂ concentrations ($1/[\text{CO}_2]$) and the $\delta^{18}\text{O}$ values of CO₂ in the plume samples ($r^2 = 0.900$, $p < 0.05$). Additionally, owing to the increase in $\Delta[\text{CO}_2]$ in 2020 ($\Delta[\text{CO}_2] = 98$ ppm) compared to that in 2019 ($\Delta[\text{CO}_2] = 61$ ppm), we obtained a significant linear correlation between $1/[\text{CO}_2]$ and the $\delta^{13}\text{C}$ values of CO₂ in the plume samples ($r^2 = 0.475$, $p < 0.05$). Such a significant linear correlation was not found in 2019 (Shingubara et al., 2021).

As clearly presented in the linear correlation between $1/[\text{CO}_2]$ and the stable isotopic compositions, all data were plotted on almost the same line irrespective of the target of sampling (main vent or southern fumaroles). This implied that either: 1) the stable isotopic compositions of fumarolic CO₂ were homogeneous irrespective of the sampling targets (main vent or southern fumaroles) in the crater; or 2) the plumes were well mixed within the semi-closed crater.

By extrapolating the regression line for the plume/air samples to the intercept (**Figures 7A,B**), the isotopic compositions of the fumarolic CO₂ were estimated to be $-3.58 \pm 0.85\text{‰}$ and $+22.01 \pm 0.68\text{‰}$ for $\delta^{13}\text{C}$ and $\delta^{18}\text{O}$, respectively. Compared with the $\delta^{18}\text{O}$ value of fumarolic CO₂ in the caldera determined in 2019 ($+16.7 \pm 6.6\text{‰}$), the precision of the endmember $\delta^{18}\text{O}$ value of fumarolic CO₂ improved dramatically, owing to the increase in $\Delta[\text{CO}_2]$ in 2020 compared to that in 2019. Dramatic improvement in the precision was obtained for the $\delta^{13}\text{C}$ value of fumarolic CO₂ as well.

The $\delta^{13}\text{C}$ value of fumarolic CO₂ in the caldera coincided well with those determined for fumarolic CO₂ ejected from subduction zone volcanoes with outlet temperatures greater than 100°C; the values ranged from -8.5 to -2.0‰ (Sano and Marty, 1995; Symonds et al., 2003). We concluded that SelPS can be utilized to determine precise $\delta^{13}\text{C}$ values of fumarolic CO₂ in eruptive volcanoes worldwide, where the direct sampling of fumarolic CO₂ is neither practical nor safe. Moreover, temporal changes in the extent of magma degassing can also be clarified based on the temporal changes in the $\delta^{13}\text{C}$ value of fumarolic CO₂, determined precisely through the repeated sampling of concentrated volcanic plume samples using SelPS.

AET_D Vs. AET₁₈₀

The $\delta^{18}\text{O}$ value of fumarolic CO₂ in the crater ($+22.01 \pm 0.68\text{‰}$) corresponds to an AET₁₈₀ of $266 \pm 65^\circ\text{C}$ (**Table 2**), assuming oxygen isotope exchange equilibrium with magmatic H₂O ($\delta^{18}\text{O} = +6.0 \pm 3.0\text{‰}$). The temperature was significantly lower than the AET_D ($629 \pm 32^\circ\text{C}$) determined in this study (**Table 2**), assuming hydrogen isotope exchange equilibrium between fumarolic H₂ ($\delta^2\text{H} = -239 \pm 6\text{‰}$) and magmatic H₂O ($\delta^2\text{H} = -24.5 \pm 7.3\text{‰}$). Assuming groundwater H₂O around the volcano ($\delta^{18}\text{O} = -8.3 \pm 0.4\text{‰}$ and $\delta^2\text{H} = -53 \pm 3\text{‰}$; Kagabu et al., 2011) instead of magmatic H₂O as H₂O that had been under the oxygen and hydrogen isotope exchange equilibrium with CO₂ and H₂, AET₁₈₀ became lower than the present estimate, while AET_D was almost the same (AET₁₈₀ = $120 \pm 8^\circ\text{C}$ and AET_D = $696 \pm 26^\circ\text{C}$; **Table 2**). We concluded that the AET₁₈₀ was significantly lower than the AET_D in the crater, at least during our observation in 2020.

TABLE 2 | Isotopic compositions of fumarolic H₂ and CO₂ estimated from the plume samples, together with apparent equilibrium temperatures calculated assuming hydrogen isotope exchange equilibrium between H₂ and H₂O (AET_D) and oxygen isotope exchange equilibrium between CO₂ and H₂O (AET_{18O}). In addition to the isotope exchange equilibrium with magmatic H₂O, that with meteoric H₂O is presented for comparison.

	1,000 δ ² H		AET _D (°C)	1,000 δ ¹⁸ O		AET _{18O} (°C)
	H ₂	H ₂ O		CO ₂	H ₂ O	
Magmatic H ₂ O	-239 ± 6	-24.5 ± 7.3	629 ± 32	+22.0 ± 0.7	+6 ± 3	266 ± 65
Meteoric H ₂ O	ditto	-53 ± 3	696 ± 26	ditto	-8.3 ± 0.4	120 ± 8

Based on the comparison between the outlet temperature determined directly in the summit fumaroles and AET_D determined from the δ²H values of H₂ in the volcanic plume ejected from summit fumaroles in the Satsuma-Iwo volcano (Japan) wherein major fumaroles are accessible, Tsunogai et al. (2013) found that, while the AET_D determined from the δ²H values of H₂ in the volcanic plume (more than 700°C) corresponds to the highest outlet temperature within the summit fumaroles at various temperatures, most summit fumaroles at Satsuma-Iwo volcano showed temperatures close to 100°C (the boiling point of water). As the hydrogen isotope exchange reaction between H₂ and H₂O is quenched at temperatures less than 200°C (Mizutani, 1983; Tsunogai et al., 2011; Tsunogai et al., 2013), the sudden cooling of the magmatic gas just beneath the summit crater in contact with groundwater should be responsible for the discrepancy between the AET_D determined from the δ²H values of H₂ in the volcanic plume as a whole and the actual outlet temperature in most fumaroles showing temperatures close to the boiling point. Conversely, Chiodini et al. (2000) found that AET_{18O} corresponded with the outlet temperature in each fumarole, which could be as low as 80°C. This implies that the oxygen isotope exchange reaction between CO₂ and H₂O was rapid at temperatures as low as 80°C.

The temperatures of fumaroles located at the bottom of the Nakadake crater determined remotely using an IR thermometer on October 2020 were as high as 348°C in the southern fumaroles (Japan Meteorological Agency, 2020). The temperature determined remotely using an IR thermometer corresponds to the lower limit temperature of the fumarole showing the highest outlet temperature within the fumarolic area (Tsunogai et al., 2011). In addition, the temperature determined remotely using an IR thermometer was higher than the temperature quenching the hydrogen isotope exchange reaction between H₂ and H₂O (Tsunogai et al., 2011). Thus, we concluded that the determined AET_D (629 ± 32°C or more) reflected the highest outlet temperature within the fumaroles in the Nakadake crater. On the other hand, the observed AET_{18O} was significantly lower than the AET_D in the crater, suggesting that the outlet temperatures of the fumaroles were heterogeneous in the Nakadake crater. This was probably attributed to the sudden cooling of the magmatic gas just beneath the crater in contact with groundwater, as schematically shown in **Figure 8**. While the temperature was close to the AET_D (approximately 630°C or more) just prior interacting with ground water, most fumarolic gases were cooled to the temperatures around the boiling point; thus, the AET_{18O} dropped to temperatures as low as 120 ± 8°C (**Figure 8**).

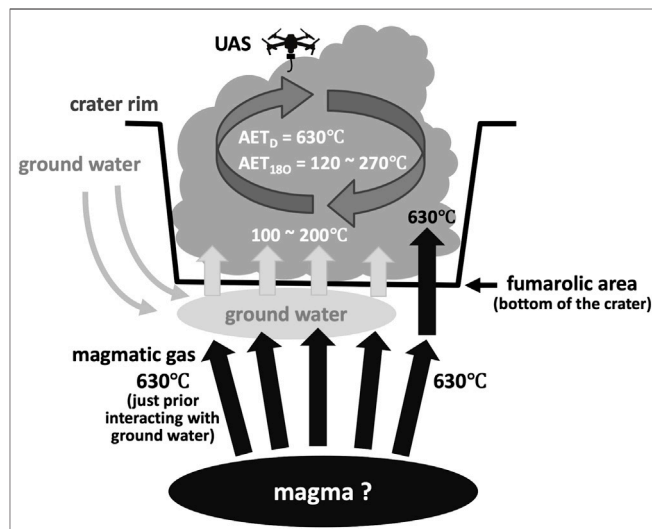


FIGURE 8 | Schematic diagram showing the cooling processes of the magmatic gas in the Nakadake crater, Aso volcano, to explain the observed discrepancy between AET_D (630°C or more) and AET_{18O} (from 120 to 270°C) determined from the volcanic plume. While the AET_D reflected the highest outlet temperature within the fumaroles in the crater, the observed AET_{18O} significantly lower than the AET_D implied that the outlet temperatures were lower than the AET_D in most of the fumaroles in the crater, probably due to the sudden cooling of the magmatic gas just beneath the crater in contact with ground water.

As demonstrated in this study, the precise and simultaneous determination of both the AET_{18O} and AET_D in eruptive volcanoes can provide novel information on each volcano, such as the physicochemical conditions of magma degassing and the development of fluid circulation systems beneath each volcano. Monitoring temporal changes is also useful for forecasting volcanic eruptions. Consequently, we should increase the opportunities to collect concentrated plume samples using SelPS attached to UAS in other eruptive volcanoes of the world, wherein major fumaroles are inaccessible.

CONCLUDING REMARKS

In this study, we improved our drone-borne automatic volcanic plume sampler, SelPS, and obtained concentrated volcanic plume samples ejected from the Nakadake crater, Aso volcano. We showed that the concentrations of both H₂ and CO₂ were higher than those collected manually in flasks at the crater rim. Additionally, we estimated the δ²H of fumarolic H₂, and both δ¹⁸O and δ¹³C of

fumarolic CO₂ precisely, based on the significant linear correlation between the reciprocal of concentrations and isotopic compositions in the plume samples. Using the $\delta^2\text{H}$ of fumarolic H₂ and $\delta^{18}\text{O}$ of fumarolic CO₂, we successfully estimated the apparent equilibrium temperatures with magmatic H₂O simultaneously and precisely for the first time in eruptive volcanoes, assuming isotope exchange equilibrium between H₂ and H₂O for $\delta^2\text{H}$ (AET_D) and between CO₂ and H₂O for $\delta^{18}\text{O}$ ratios (AET_{18O}). We found that the AET_{18O} was significantly lower than the AET_D. While the temperature was 630°C or more originally, most fumarolic gases were cooled to the temperature around the boiling point just beneath the crater in the volcano. Simultaneous and precise determination of both the AET_{18O} and AET_D in eruptive volcanoes can provide novel information on each volcano, such as the physicochemical conditions of magma degassing and the development of fluid circulation systems beneath each volcano. Monitoring temporal changes is also useful and we should increase the collection of plume samples using SeIPS attached to UAS in other eruptive volcanoes, wherein major fumaroles are inaccessible.

DATA AVAILABILITY STATEMENT

The original contributions presented in the study are included in the article/**Supplementary Material**, further inquiries can be directed to the corresponding author.

AUTHOR CONTRIBUTIONS

RS developed and improved SeIPS with support from MI, YM, FN, and UT. UT and AY planned the sampling. SY, MU, and AY

designed the sampling strategy and operated the UAS. RS, MI, and YM analyzed the samples. UT wrote the manuscript with inputs from FN, RS, YM, MI, and AY. All authors read and approved the final manuscript.

FUNDING

This research was supported by MEXT (The Ministry of Education, Culture, Sports, Science, and Technology of Japan) Integrated Program for Next Generation Volcano Research and Human Resource Development (Theme B), MEXT Grant-in-aid for Scientific Research under grant numbers 16K13914 and 26610181, and the research grant from the IWATANI NAOJI foundation to UT.

ACKNOWLEDGMENTS

We thank Prof. Valerio Acocella, Prof. John Stix, and Prof. Philipson Bani for valuable suggestions and comments on the earlier version of this manuscript. The Aso Volcano Disaster Prevention Council supported our fieldwork at the Aso volcano. We also appreciate the support from the Research Equipment Development Group of Equipment Development Support Section, Technical Center, Nagoya University.

SUPPLEMENTARY MATERIAL

The Supplementary Material for this article can be found online at: <https://www.frontiersin.org/articles/10.3389/feart.2022.833733/full#supplementary-material>

REFERENCES

- Aiuppa, A., Federico, C., Giudice, G., and Gurrieri, S. (2005). Chemical Mapping of a Fumarolic Field: La Fossa Crater, Vulcano Island (Aeolian Islands, Italy). *Geophys. Res. Lett.* 32, L13309. doi:10.1029/2005gl023207
- Aiuppa, A., Moretti, R., Federico, C., Giudice, G., Gurrieri, S., Liuzzo, M., et al. (2007). Forecasting Etna Eruptions by Real-Time Observation of Volcanic Gas Composition. *Geology* 35, 1115–1118. doi:10.1130/g24149a.1
- Cantrell, C. A. (2008). Technical Note: Review of Methods for Linear Least-Squares Fitting of Data and Application to Atmospheric Chemistry Problems. *Atmos. Chem. Phys.* 8, 5477–5487. doi:10.5194/acp-8-5477-2008
- Chiodini, G., Allard, P., Caliro, S., and Parello, F. (2000). ¹⁸O Exchange between Steam and Carbon Dioxide in Volcanic and Hydrothermal Gases: Implications for the Source of Water. *Geochim. Cosmochim. Acta* 64, 2479–2488. doi:10.1016/s0016-7037(99)00445-7
- Chiodini, G., Caliro, S., Aiuppa, A., Avino, R., Granieri, D., Moretti, R., et al. (2010). First ¹³C/¹²C Isotopic Characterisation of Volcanic Plume CO₂. *Bull. Volcanol.* 73, 531–542. doi:10.1007/s00445-010-0423-2
- Fischer, T. P., and Lopez, T. M. (2016). First Airborne Samples of a Volcanic Plume for $\delta^{13}\text{C}$ of CO₂ Determinations. *Geophys. Res. Lett.* 43, 3272–3279. doi:10.1002/2016gl068499
- Francis, P., Burton, M. R., and Oppenheimer, C. (1998). Remote Measurements of Volcanic Gas Compositions by Solar Occultation Spectroscopy. *Nature* 396, 567–570. doi:10.1038/25115
- Gerlach, T. M., and Taylor, B. E. (1990). Carbon Isotope Constraints on Degassing of Carbon Dioxide from Kilauea Volcano. *Geochim. Cosmochim. Acta* 54, 2015–2058. doi:10.1016/0016-7037(90)90270-u
- Hirabayashi, J., Oosaka, J., and Ozawa, T. (1982). Relationship Between Volcanic Activity and Chemical Composition of Volcanic Gases—A Case Study on the Sakurajima Volcano. *Geochem. J.* 16, 11–21. doi:10.2343/geochemj.16.11
- Ijiri, A., Tsunogai, U., and Gamo, T. (2003). A Simple Method for Oxygen-18 Determination of Milligram Quantities of Water Using NaHCO₃ Reagent. *Rapid Commun. Mass. Spectrom.* 17, 1472–1478. doi:10.1002/rcm.1081
- James, M., Carr, B., D'arcy, F., Diefenbach, A., Dietterich, H., Fornaciai, A., et al. (2020). Volcanological Applications of Unoccupied Aircraft Systems (UAS): Developments, Strategies, and Future Challenges. *Volcanica* 3, 67–114. doi:10.30909/vol.03.01.67114
- Japan Meteorological Agency (2020). *Monthly Report on Earthquakes and Volcanoes in Japan: October, 2020*. Tokyo: Japan Meteorological Agency.
- Kagabu, M., Shimada, J., Shimano, Y., Higuchi, S., and Noda, S. (2011). Groundwater Flow System in Aso Caldera. *Nihon Suimon Kagaku Kaishi* 41, 1–17. doi:10.4145/jahs.41.1
- Kagoshima, T., Sano, Y., Takahata, N., Ishida, A., Tomonaga, Y., Rouleau, E., et al. (2016). Spatial and Temporal Variations of Gas Geochemistry at Mt. Ontake, Japan. *J. Volcanol. Geotherm. Res.* 325, 179–188. doi:10.1016/j.jvolgeores.2016.06.013
- Kawagucci, S., Tsunogai, U., Kudo, S., Nakagawa, F., Honda, H., Aoki, S., et al. (2005). An Analytical System for Determining $\delta^{17}\text{O}$ in CO₂ Using Continuous Flow-Isotope Ratio MS. *Anal. Chem.* 77, 4509–4514. doi:10.1021/ac050266u
- Keeling, C. D. (1958). The Concentration and Isotopic Abundances of Atmospheric Carbon Dioxide in Rural Areas. *Geochim. Cosmochim. Acta* 13, 322–334. doi:10.1016/0016-7037(58)90033-4
- Komatsu, D. D., Tsunogai, U., Kamimura, K., Konno, U., Ishimura, T., and Nakagawa, F. (2011). Stable Hydrogen Isotopic Analysis of Nanomolar Molecular Hydrogen by Automatic Multi-step Gas Chromatographic Separation. *Rapid Commun. Mass. Spectrom.* 25, 3351–3359. doi:10.1002/rcm.5231

- Liu, E. J., Aiuppa, A., Alan, A., Arellano, S., Bitetto, M., Bobrowski, N., et al. (2020). Aerial Strategies advance Volcanic Gas Measurements at Inaccessible, Strongly Degassing Volcanoes. *Sci. Adv.* 6, eabb9103. doi:10.1126/sciadv.abb9103
- Mizutani, Y. (1983). Deuterium Fractionation between Water Vapor and Hydrogen Gas in Fumarolic Gases. *Geochem. J.* 17, 161–164. doi:10.2343/geochemj.17.161
- Mori, T., Notsu, K., Tohjima, Y., and Wakita, H. (1993). Remote Detection of HCl and SO₂ in Volcanic Gas from Unzen Volcano, Japan. *Geophys. Res. Lett.* 20, 1355–1358. doi:10.1029/93gl01065
- Ohba, T., Hirabayashi, J.-i., and Yoshida, M. (1994). Equilibrium Temperature and Redox State of Volcanic Gas at Unzen Volcano, Japan. *J. Volcanol. Geotherm. Res.* 60, 263–272. doi:10.1016/0377-0273(94)90055-8
- Ohba, T., Yaguchi, M., Nishino, K., Numanami, N., Daita, Y., Sukigara, C., et al. (2019). Time Variations in the Chemical and Isotopic Composition of Fumarolic Gases at Hakone Volcano, Honshu Island, Japan, over the Earthquake Swarm and Eruption in 2015, Interpreted by Magma Sealing Model. *Earth Planets Space* 71, 48. doi:10.1186/s40623-019-1027-5
- Ohba, T., Yaguchi, M., Tsunogai, U., Ito, M., and Shingubara, R. (2021). Behavior of Magmatic Components in Fumarolic Gases Related to the 2018 Phreatic Eruption at Ebinokogen Ioyama Volcano, Kirishima Volcanic Group, Kyushu, Japan. *Earth Planets Space* 73, 81. doi:10.1186/s40623-021-01405-4
- Ossaka, J., Ozawa, T., Nomara, T., Ossaka, T., Hirabayashi, J., Takaesu, A., et al. (1980). Variation of Chemical Compositions in Volcanic Gases and Water at Kusatsu-Shirane Volcano and its Activity in 1976. *Bull. Volcanol.* 43, 207–216. doi:10.1007/bf02597622
- Peters, W., Van Der Velde, I. R., Van Schaik, E., Miller, J. B., Ciaia, P., Duarte, H. F., et al. (2018). Increased Water-Use Efficiency and Reduced CO₂ Uptake by Plants during Droughts at a continental Scale. *Nat. Geosci.* 11, 744–748. doi:10.1038/s41561-018-0212-7
- Price, H., Jaeglé, L., Rice, A., Quay, P., Novelli, P. C., and Gammon, R. (2007). Global Budget of Molecular Hydrogen and its Deuterium Content: Constraints from Ground Station, Cruise, and Aircraft Observations. *J. Geophys. Res.* 112, D22. doi:10.1029/2006jd008152
- Rice, A., Quay, P., Stutsman, J., Gammon, R., Price, H., and Jaeglé, L. (2010). Meridional Distribution of Molecular Hydrogen and its Deuterium Content in the Atmosphere. *J. Geophys. Res.* 115, D12306. doi:10.1029/2009jd012529
- Richet, P., Bottinga, Y., and Javoy, M. (1977). A Review of Hydrogen, Carbon, Nitrogen, Oxygen, Sulphur, and Chlorine Stable Isotope Fractionation Among Gaseous Molecules. *Annu. Rev. Earth Planet. Sci.* 5, 65–110. doi:10.1146/annurev.earth.05.050177.000433
- Rizzo, A. L., Jost, H. J., Caracausi, A., Paonita, A., Liotta, M., and Martelli, M. (2014). Real-time Measurements of the Concentration and Isotope Composition of Atmospheric and Volcanic CO₂ at Mount Etna (Italy). *Geophys. Res. Lett.* 41, 2382–2389. doi:10.1002/2014gl059722
- Sambuichi, T., Tsunogai, U., Kura, K., Nakagawa, F., and Ohba, T. (2021). High-precision $\Delta^{17}\text{O}$ Measurements of Geothermal H₂O and MORB on the VSMOW-SLAP Scale: Evidence for Active Oxygen Exchange between the Lithosphere and Hydrosphere. *Geochem. J.* 55, e25–e33. doi:10.2343/geochemj.2.0644
- Sano, Y., and Marty, B. (1995). Origin of Carbon in Fumarolic Gas from Island Arcs. *Chem. Geology.* 119, 265–274. doi:10.1016/0009-2541(94)00097-r
- Sasakawa, M., Tsunogai, U., Kameyama, S., Nakagawa, F., Nojiri, Y., and Tsuda, A. (2008). Carbon Isotopic Characterization for the Origin of Excess Methane in Subsurface Seawater. *J. Geophys. Res.* 113, C03012. doi:10.1029/2007jc004217
- Schipper, C. L., Moussallam, Y., Curtis, A., Peters, N., Barnie, T., Bani, P., et al. (2017). Isotopically ($\delta^{13}\text{C}$ and $\delta^{18}\text{O}$) Heavy Volcanic Plumes from Central Andean Volcanoes: a Field Study. *Bull. Volcanol.* 79. doi:10.1007/s00445-017-1146-4
- Shingubara, R., Tsunogai, U., Ito, M., Nakagawa, F., Yoshikawa, S., Utsugi, M., et al. (2021). Development of a Drone-Borne Volcanic Plume Sampler. *J. Volcanol. Geotherm. Res.* 412, 107197. doi:10.1016/j.jvolgeores.2021.107197
- Shinohara, H., Kazahaya, K., Saito, G., Matsushima, N., and Kawanabe, Y. (2002). Degassing Activity from Iwodake Rhyolitic Cone, Satsuma-Iwojima Volcano, Japan: Formation of a New Degassing Vent, 1990–1999. *Earth Planets Space* 54, 175–185. doi:10.1186/bf03353017
- Shinohara, H., Yokoo, A., and Kazahaya, R. (2018). Variation of Volcanic Gas Composition during the Eruptive Period in 2014–2015 at Nakadake Crater, Aso Volcano, Japan. *Earth Planets Space* 70, 151. doi:10.1186/s40623-018-0919-0
- Shinohara, H., Kazahaya, R., Ohminato, T., Kaneko, T., Tsunogai, U., and Morita, M. (2020). Variation of Volcanic Gas Composition at a Poorly Accessible Volcano: Sakurajima, Japan. *J. Volcanol. Geotherm. Res.* 407, 107098. doi:10.1016/j.jvolgeores.2020.107098
- Shinohara, H. (2005). A New Technique to Estimate Volcanic Gas Composition: Plume Measurements with a Portable Multi-Sensor System. *J. Volcanol. Geotherm. Res.* 143, 319–333. doi:10.1016/j.jvolgeores.2004.12.004
- Stix, J., and de Moor, J. M. (2018). Understanding and Forecasting Phreatic Eruptions Driven by Magmatic Degassing. *Earth Planets Space* 70, 83. doi:10.1186/s40623-018-0855-z
- Stoiber, R. E., and Jepsen, A. (1973). Sulfur Dioxide Contributions to the Atmosphere by Volcanoes. *Science* 182, 577–578. doi:10.1126/science.182.4112.577
- Symonds, R. B., Poreda, R. J., Evans, W. C., Janik, C. J., and Ritchie, B. E. (2003). Mantle and Crustal Sources of Carbon, Nitrogen, and Noble Gases in Cascade-Range and Aleutian-Arc Volcanic Gases. United States Geological Survey Open-File Report 2003-436. Reston, VA: U.S. Geological Survey. doi:10.3133/ofr03436
- Taran, Y. A., Hedenquist, J. W., Korzhinsky, M. A., Tkachenko, S. I., and Shmulovich, K. I. (1995). Geochemistry of Magmatic Gases from Kudryavy Volcano, Iturup, Kuril Islands. *Geochim. Cosmochim. Acta* 59, 1749–1761. doi:10.1016/0016-7037(95)00079-f
- Tohjima, Y., Katsumata, K., Morino, I., Mukai, H., Machida, T., Akama, I., et al. (2009). Theoretical and Experimental Evaluation of the Isotope Effect of NDIR Analyzer on Atmospheric CO₂ Measurement. *J. Geophys. Res.* 114, D13302. doi:10.1029/2009jd011734
- Tsunematsu, K., Ishii, K., and Yokoo, A. (2019). Transport of Ballistic Projectiles during the 2015 Aso Strombolian Eruptions. *Earth Planets Space* 71, 49. doi:10.1186/s40623-019-1029-3
- Tsunogai, U., Hachisu, Y., Komatsu, D. D., Nakagawa, F., Gamo, T., and Akiyama, K.-i. (2003). An Updated Estimation of the Stable Carbon and Oxygen Isotopic Compositions of Automobile CO Emissions. *Atmos. Environ.* 37, 4901–4910. doi:10.1016/j.atmosenv.2003.08.008
- Tsunogai, U., Kamimura, K., Anzai, S., Nakagawa, F., and Komatsu, D. D. (2011). Hydrogen Isotopes in Volcanic Plumes: Tracers for Remote Temperature Sensing of Fumaroles. *Geochim. Cosmochim. Acta* 75, 4531–4546. doi:10.1016/j.gca.2011.05.023
- Tsunogai, U., Komatsu, D. D., and Nakagawa, F. (2013). Remote Temperature Sensing on Volcanic Fumaroles Using HIReTS: Applications to Satsuma-Iwojima Volcano, Japan. *Bull. Volcanol. Soc. Jpn.* 58, 443–459. doi:10.18940/kazan.58.3_443
- Tsunogai, U., Cheng, L., Ito, M., Komatsu, D. D., Nakagawa, F., and Shinohara, H. (2016). Remote Determinations on Fumarole Outlet Temperatures in an Eruptive Volcano. *Geophys. Res. Lett.* 43, 11620–11627. doi:10.1002/2016gl070838
- Tsunogai, U., Miyoshi, Y., Matsushita, T., Komatsu, D. D., Ito, M., Sukigara, C., et al. (2020). Dual Stable Isotope Characterization of Excess Methane in Oxidic Waters of a Mesotrophic lake. *Limnol. Oceanogr.* 65, 2937–2952. doi:10.1002/lno.11566
- Welp, L. R., Keeling, R. F., Meijer, H. A. J., Bollenbacher, A. F., Piper, S. C., Yoshimura, K., et al. (2011). Interannual Variability in the Oxygen Isotopes of Atmospheric CO₂ Driven by El Niño. *Nature* 477, 579–582. doi:10.1038/nature10421
- Yokoo, A., Ishii, K., Ohkura, T., and Kim, K. (2019). Monochromatic Infrasound Waves Observed during the 2014–2015 Eruption of Aso Volcano, Japan. *Earth Planets Space* 71, 12. doi:10.1186/s40623-019-0993-y
- York, D. (1969). Least Squares Fitting of a Straight Line with Correlated Errors. *Earth Planet. Sci. Lett.* 5, 320–324.

Conflict of Interest: The authors declare that the research was conducted in the absence of any commercial or financial relationships that could be construed as a potential conflict of interest.

Publisher's Note: All claims expressed in this article are solely those of the authors and do not necessarily represent those of their affiliated organizations, or those of the publisher, the editors and the reviewers. Any product that may be evaluated in this article, or claim that may be made by its manufacturer, is not guaranteed or endorsed by the publisher.

Copyright © 2022 Tsunogai, Shingubara, Morishita, Ito, Nakagawa, Yoshikawa, Utsugi and Yokoo. This is an open-access article distributed under the terms of the Creative Commons Attribution License (CC BY). The use, distribution or reproduction in other forums is permitted, provided the original author(s) and the copyright owner(s) are credited and that the original publication in this journal is cited, in accordance with accepted academic practice. No use, distribution or reproduction is permitted which does not comply with these terms.